Rational Pathways to Ordered Multi-Anion Chalcogenides Using Retrosynthetic Crystal Chemistry

Ayat Tassanov[†], Huiju Lee[§], Yi Xia[§], and James M. Hodges[†*]

[†] Department of Chemistry, The Pennsylvania State University, University Park, Pennsylvania 16802, United States.

[§] Department of Mechanical and Materials Engineering, Portland State University, Portland, Oregon 97201, United States.

KEYWORDS. Synthesis, Chalcogenides, Mixed-Anion, Crystal Structure

ABSTRACT: Mixed-anion chalcogenides are a versatile class of materials with properties that can be fine-tuned for specific applications. While chalcogen anions (Q = S, Se, Te) tend to form solid solutions in simple binary systems, ordering does occur in structures that have more than one unique anion site. Here, we use crystallographic analysis and hard-soft acid-base principles to predict the Wyckoff positions that secondary chalcogens will occupy in a range of single-anion hosts. The analysis serves as a guide for generating ordered sulfoselenide, selenotelluride, and sulfotelluride products in a predictable manner. The study focuses on ternary and quaternary systems with varying compositional and structural features, with an emphasis on 3D $CsCu_5Q_3$ ($P4_2/mnm$) and 2D $NaCuZrQ_3$ ($Pnma$) crystal systems. The samples were prepared using high-temperature solid-state methods and structurally characterized using single-crystal X-ray diffraction. Ordering in the mixed-anion products is attributed to size and bonding variance across the chalcogen series. The degree of ordering varies according to the distinctiveness of the local chemistry at the anion sites and additionally, the specific combination of chalcogens employed in the reaction. Additionally, we find that mixed-chalcogen products can adopt phases that are distinct from their single-anion end members, including $KCuZrTe_2S$ ($P2_1m$), where an alternate arrangement of polyhedral building blocks maximizes favorable bonding interactions. Density-functional theory calculations corroborate the experimental findings and offer additional insights into the ordering trends. We anticipate that the reverse-engineering approach, which is inspired by the retrosynthetic analyses used in molecular chemistry, will help accelerate the discovery and understanding of heteroanionic phenomena.

INTRODUCTION

The discovery of new materials drives advances in technology and is a central goal in the field of solid state chemistry.[1-3] To this end, an assortment of synthetic strategies have emerged in recent years that can be used to generate materials with targeted features and properties.[4-7] Such efforts have translated to advances in various applications including energy storage,[8-10] catalysis,[11-13] and photovoltaics.[14-16] Still, serendipity continues to play an oversized role in exploratory research. Advanced strategies that deliver atomically precise solids in a more efficient manner are needed for the next-generation of applications.

Metal chalcogenides are among the most structurally diverse classes of materials.[17-19] They are ubiquitous in nature as minerals and serve as key components in many energy-related applications. Divalent chalcogen anions (Q^{2-} = S^{2-}, Se^{2-}, Te^{2-}) share similar bonding features and often form solid solutions in binary crystal systems. This allows their properties to be fine-tuned by simply adjusting the ratio of chalcogens employed in a synthesis. For example, the electronic structure of zincblende-type CdTe can be optimized for solar absorption by using mixed-anion $CdTe_{1-x}Se_x$ compositions.[20] This tunability is one of the reasons they are the primary absorber used in thin-film photovoltaic technologies.[21]

Although chalcogen anions form solid solutions in simple structures, ordering does occur in systems with more than one crystallographically distinct anion site.[22-26] Such ordering can have a profound influence on their properties. A notable example is the $Bi_2Te_{3-x}Se_x$ pseudo-binary system. These narrow-gap semiconductors serve as the n-type component in thermoelectric modules and have emerged as an active area in quantum materials research.[27, 28] Here, the single-anion Bi_2Te_3 and Bi_2Se_3 end members both adopt the tetradymite-type structure, which can be described as quintuple Q2-Bi-Q1-Bi-Q2 layers held together by Van der Waals interactions. Due to the distinct local chemistry at the Q1 and Q2 sites, the mixed-anion $Bi_2Te_{3-x}Se_x$ compositions do not form true solid solutions. Instead, Te anions prefer to occupy the Q2 positions at edge of the layers due to their larger size and polarizability, while Se occupies the Q2 sites that are fully coordinated to Bi^{3+} cations. The ordered configuration results in more favorable Van der Waals interactions at the interface between the layers.[29, 30] Critically, the degree of ordering can vary depending on the method of synthesis and significantly affect their properties.[31] This variability creates problems with reproducibility and makes them notoriously difficult to model accurately.[32]

Local ordering can affect the properties of extended solids in many ways but can be challenging to characterize in bulk powders.[33-36] This represents a scientific roadblock since most applications rely on polycrystalline materials. Single-crystal X-ray diffraction (SCXRD) can be an effective tool for characterizing local ordering phenomena but requires high-quality single crystals. Accordingly, we are exploring anion ordering in laboratory-grown crystals with a range of structural and compositional features in order to establish a framework for predicting when and how ordering will occur. This information augments existing frameworks used in materials optimization, while simultaneously delivering model substrates for studying latent structure-property relationships.

A survey of the existing literature suggests that basic bonding principles can be effective descriptors for predicting how anions will segregate on a given sublattice.[37-39] Here, we exploit this feature to reverse-engineer ordered sulfoselenide, selenotelluride, and sulfotelluride products in a predictable manner. Single-anion hosts with targeted features are first identified from the structural database. Crystallographic analysis is then used to predict the Wyckoff position each chalcogen will prefer to occupy in a given mixture of anions. The analysis is used as a guide for generating ordered, mixed-chalcogen solids with predetermined arrangements of atoms and bonding motifs. Here, we draw analogy to the retrosynthetic analyses used in organic chemistry, which provide rational pathways to molecules with targeted bonds and functionality.

Compared to metal oxides, the chalcogenides have relatively low melting points and can be synthesized directly through high-temperature methods.[17] This feature, along with their structural and compositional diversity, makes them ideal systems for substitutional studies. In this report, we systematically explore anion substitution on a series of single-chalcogen parent structures. Priority is given to metal selenide hosts, since Se^{2-} has intermediate size and electronegativity among the chalcogen series. This affords more substitutional degrees of freedom, but the technique is also applicable to sulfide and telluride structures. Particular emphasis is given to the 3D $CsCu_5Se_3$ ternary and 2D $NaCuZrSe_3$ quaternary systems, which crystallize in the $P4_2/mnm$ and $Pnma$ space groups, respectively. $CsCu_5Se_3$ has two distinct Se anions, where Se1 is four-coordinate with relatively short Se-Cu bonds and Se2 has seven Se-Cu bonds. Here, the larger chalcogen in the mixed-anion products show a strong preference for the Se2 (Q2) site, while smaller chalcogens tend to occupy Se1 (Q1) positions, in accordance with geometric constraints. Conversely, layered $NaCuZrSe_3$ has three distinct Se anions, which form polar covalent interactions with two different metal cations, Cu^+ and Zr^{4+}. Here, chalcogens in mixed-anion products reside at positions that maximize favorable bonding interactions, which is rationalized using hard-soft acid-base (HSAB) concepts. Bader charge analyses can give added insight into the ionicity of metal-chalcogen bonds and a provides a more quantitative descriptor for predicting chalcogen ordering.[40]

In most cases, sulfotelluride products are ostensibly fully ordered, but a range of order-disorder behavior is observed in the sulfoselenide and selenotelluride products. The degree of ordering correlates with the distinctiveness of the anion sites within the host structure, as well as the relative size of the two chalcogens. The latter trend is analogous to the Hume-Rothery rules used to predict ordering in intermetallics.[41] Motivated by this observation, we employ a long-range ordering parameter η to quantify the ordering trends. Interestingly, we find that sulfotellurides can crystallize in structures not found in their single-anion end members. This is highlighted in 2D $KCuZrTe_2S$, which adopts the $P2_1m$ space group, while all three single-anion analogues crystallize in the alternate $Cmcm$ structure. Here, the alternate arrangement of tetrahedral and polyhedral building blocks in the $P2_1m$ phase enables more energetically favorable chalcogen-metal bonding interactions.

Density-functional theory calculations (DFT) are used to compare the stability of the ordered and (hypothetical) disordered systems. Here, to model disorder, we systematically vary the positions of the anions within the unit cell and calculate the total energy of all the configurations. The average of these values is then compared to the total energy of the experimentally determined configuration. The difference in these values is dubbed “switching energy”, where large switching energies are found to correlate with greater levels of ordering. The approach circumvents the need for expensive supercell calculations and provides a semi-quantitative tool for predicting ordering behavior in mixed-chalcogen compounds.

It is interesting to note that true solid solution behavior is not observed in *any* of the mixed-anion systems we have studied. This is surprising, considering this is rarely discussed in the literature and the importance of chalcogenides in industry. This report aims to draw attention to this latent phenomena and additionally, demonstrate how it can be exploited as a synthetic tool. Although the focus of the study is chalcogenides, we believe the analysis will prove applicable to other classes of materials.

RESULTS

Chalcogen Ordering in Tetragonal $CsCu_5Q_3$. Mixed-chalcogen $CsCu_5Q_2Q'$ (Q' = lighter chalcogen) compounds were prepared using high-temperature solid-state reactions. Briefly, stoichiometric amounts of elemental and Cs_2Q binary precursors were loaded into carbon-coated quartz tubes and then flame-sealed under dynamic vacuum. The reaction vessels were heated to 1123 K in a box furnace, dwelled for 6 h, then radiatively cooled in the furnace. Black plate-like crystals suitable for SCXRD were isolated from the ingot products. Full synthetic details can be found in the experimental section.

$CsCu_5Se_3$ was previously reported to crystallize in the tetragonal $P4_2/mnm$ space group and belongs to a larger family of compounds that adopt the $CsAg_5Te_3$-type structure.[42] Several compounds with this structural archetype have been reported to have excellent thermoelectric performance, including $CsCu_5Se_3$, which was part of our motivation for working with this system.[42-44] $CsCu_5Se_3$ was re-synthesized and structurally characterized using SCXRD. Information regarding the structural refinement and crystallographic data tables can be found in the Supporting Information. The asymmetric unit for $CsCu_5Se_3$ has 1 Cs atom, 3

Cu atoms, and 2 Se atoms. The structure is composed of distorted trigonal $CuSe_3$ and tetrahedral $CuSe_4$ units, which connect to form a 3D anionic framework with 1D pores containing counterbalancing Cs^+ cations (Figure 1A). The two distinct Se atoms exhibit different coordination geometries, where Se1 and Se2 form four and seven bonds with Cu, respectively. The Se-Cu bond distances are listed in Table 1.

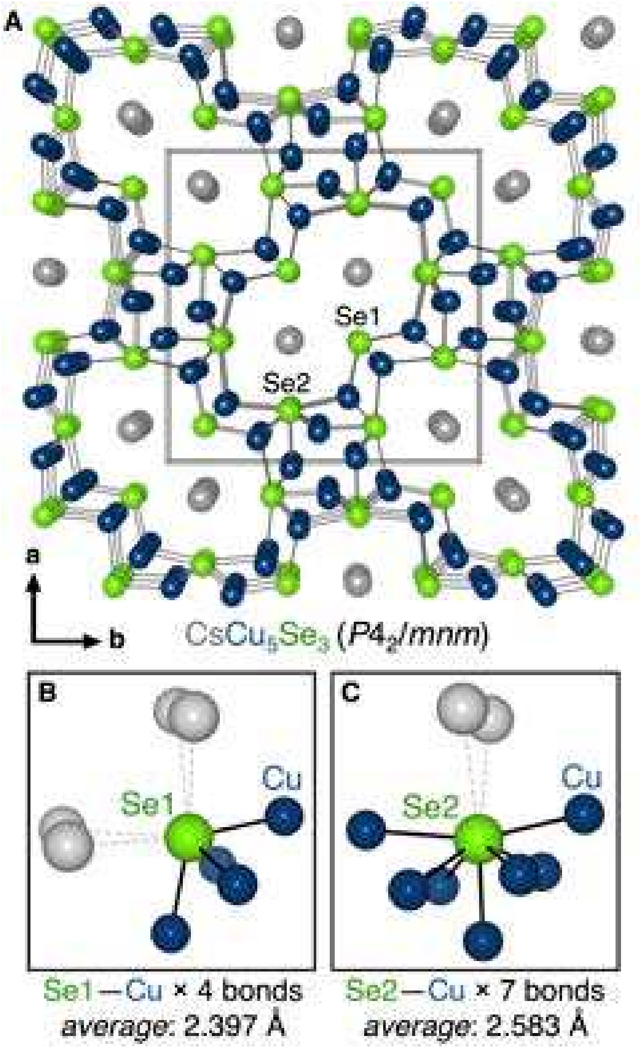

Figure 1. (A) Crystal structure of $CsCu_5Se_3$ viewed along the c-axis. The structure contains two distinct Se sites, where (B) Se1 forms four Cu-Se bonds and (C) Se2 forms seven Cu-Se bonds. Ionic Se-Cs interactions are shown as dotted lines. Cs atoms are depicted in light grey, Cu atoms in blue, and Se atoms in green.

Figure 1B shows the coordination environment at the Se1 anion, which forms four relatively short Se-Cu bonds with an average length of 2.397 Å. The Se1 anions interact with four Cs^+ cations with interatomic distances of 3.620 Å, which are longer than in Cs_2Se.[45] The coordination for Se2 is illustrated in Figure 1C, showing seven Se-Cu bonds with an average length of 2.583 Å. Here, Se2 interacts with two Cs^+ cations that have interatomic distances of 3.585 Å, which are also shorter than in Cs_2Se. From a geometric perspective, intuition suggests that Se2 is the larger of the two sites, since it has a higher coordination number and longer Se-Cu bonds.

Bond Valence sum (BVS) values were calculated and can be found in Table S1. Here, Se1 and Se2 anions have BVS values of 1.75, and 1.54, respectively. We note that although both values are less than 2, BVS deficiency at chalcogen sites within Cu-containing compounds is not uncommon.[46] BVS deficiency (or residual valence) can occur when ions are located at crystallographic sites that too large for its bonds to adopt their ideal length.[47] Hence, the smaller BVS value at the Se2 site could be taken as additional evidence that it is the larger of the two anion sites. We note that there are other possible interpretations of this data, and accordingly, this data is only used to augment the other analyses.

Bader charge analysis is used to further assess the bonding character at the distinct chalcogen sites.[48] The analysis is used to estimate how electron density is distributed throughout the $CsCu_5Se_3$ lattice, and proves be a useful tool for evaluating the ionicity of the Se-metal bonds. Calculated Bader charge values for the atoms in $CsCu_5Se_3$ are tabulated in Figure S2. Here, we see the formally monovalent Cs cations have an approximate charge of +0.74, which is more than twice the value of the monovalent Cu atoms. The greater degree of ionicity in the Cs-Se interactions compared to Cu-Se is expected considering the large difference in electronegativity of the two metals.[49] Meanwhile, Se1 and Se2 have calculated Bader charges of -0.75 and -0.63, respectively. The greater charge at the Se1 site is interpreted as greater ionicity at this site and accordingly, the Se1 site is expected to be the preferred site of the more electronegative chalcogen in a mixed-anion product.[50]

Table 1. Selected Selenium-Metal Interatomic Distances in the $CsCu_5Se_3$ Structure

atom pair	bond distance (Å)	atom pair	bond distance (Å)
Se**1**–Cu2	2.3823(15) × 2	Se**2**–Cu2	2.5772(15)
Se**1**–Cu3	2.4114(8) × 2	Se**2**–Cu2	2.6659(10) × 2
Se**1**···Cs1	3.6200(7) × 4	Se**2**–Cu3	2.7247(16)
Se**2**–Cu1	2.4088(11)	Se**2**···Cs1	3.5851(6) × 2
Se**2**–Cu1	2.5203(8) × 2		

The chemical formula for $CsCu_5Se_3$ contains one Se1 atom and two Se2 atoms. Accordingly, the substitution experiments described below targeted products with a nominal $CsCu_5Q_2Q'$ composition, where Q' represents the smaller (lighter) of the two chalcogens. Hence, the nominal anion composition in the products is 67% Q and 33% Q', which is also the expected occupancy at each site on the anion sublattice in a perfect solid solution.

$CsCu_5Se_2S$ and $CsCu_5Te_2Se$ products are found to crystallize in the same $P4_2/mnm$ space group as the parent selenide, and the structures are shown in panels A and B of Figure 2, respectively. The $CsCu_5Te_2S$ sulfotelluride product also adopts the tetragonal structure and is shown in Figure 2C, representing a complete replacement of the Se sublattice. We note that the pure telluride and sulfide end members of this structure are not reported, and attempts to synthesize these analogues were unsuccessful. SCXRD data for the three mixed-chalcogen compounds are shown in Table S3 along with information regarding structural refinements.

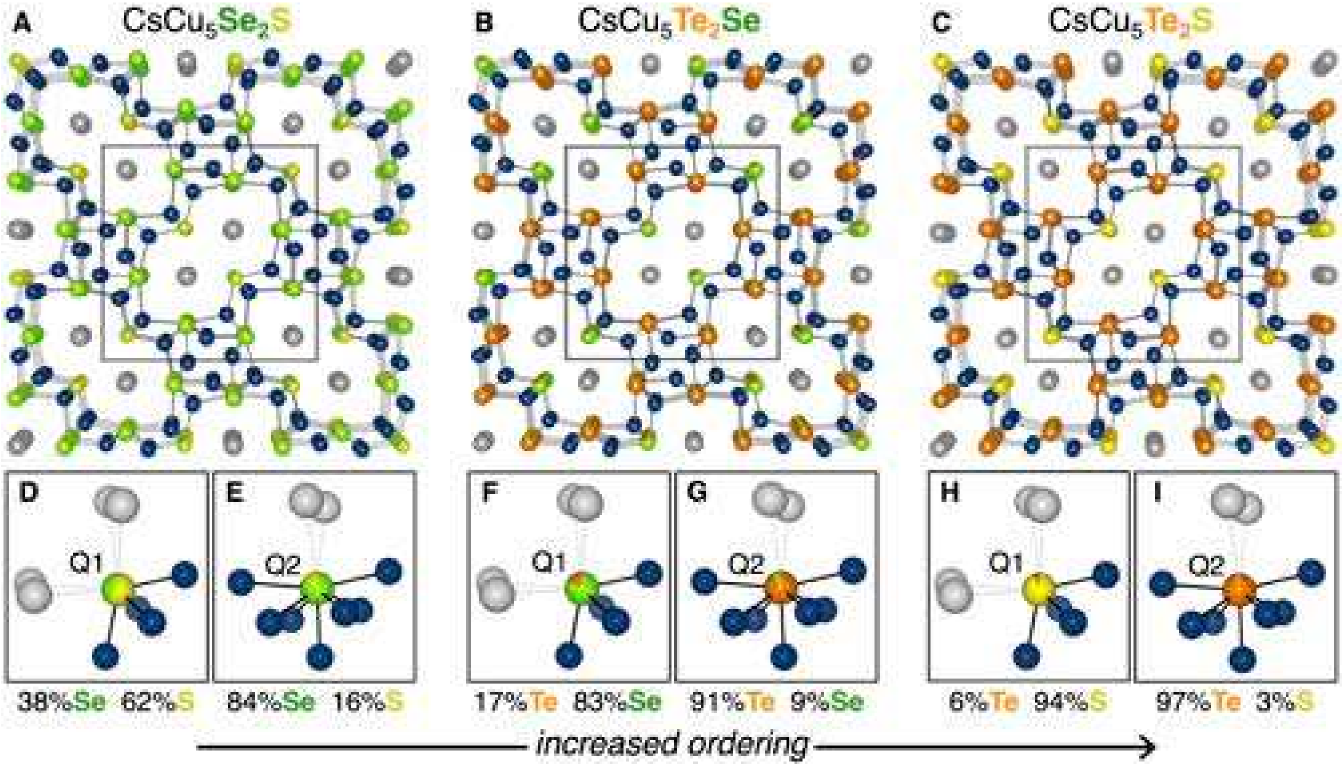

Figure 2. Crystal structure of (A) $CsCu_5Se_2S$, (B) $CsCu_5Te_2Se$, and (C) $CsCu_5Te_2S$ with the tetragonal $P4_2/mnm$ space group viewed along the c-axis. The corresponding chalcogen coordination at the Q1 and Q2 sites is shown below each structure (panels D through I). Chalcogen atoms are depicted as pie charts to illustrate the occupancy at each site, and the percent occupancy from the structural refinements is shown for clarity. Cs atoms are depicted in light grey, Cu atoms in blue, S atoms in yellow, Se atoms in green, and Te atoms in orange.

Chalcogen coordination at the Q1 and Q2 sites for the three mixed-chalcogen products are shown in panels D through I in Figure 2. Here, Q atoms are depicted as pie-charts to illustrate the occupancy of each chalcogen at the distinct sublattice sites. The refined occupancy at the Q1 site in $CsCu_5Se_2S$ is 62% S (38% Se) and Q2 is 84% Se (16% S). These values deviate significantly from solid solution behavior and indicate S^{2-} and Se^{2-} anions prefer to occupy the Q1 and Q2 sites, respectively. The degree of segregation is observed to be greater in the $CsCu_5Te_2Se$ product, where Q1 is 83% Se (17% Te) and Q2 is 91% Te (9% Se). The $CsCu_5Te_2S$ product, where the selenide sublattice is completely replaced with tellurium and sulfur, is ostensibly fully ordered. Here, Q1 is 94% S (6% Te) and Q2 is 97% Te (3% S). The increase in ordering across the series of mixed-chalcogen permutations is attributed to the relative size of the anion radii in the products,[51] and is a general trend found in all of the studied systems.

Ordering in extended solids that correlates with atomic radii is a well-studied phenomenon in the metallurgical sciences. Hume-Rothery was among the first to develop a chemical framework for predicting ordering behavior in mixed-metal solids.[41] The framework is based on the relative size of the metal radii, as well as their valency and electronegativity. Metals with similar size (less than 15% difference) and electronic properties tend to form solid solutions, while dissimilar metals will segregate to form ordered intermetallic phases. Intermetallics exhibit varying degrees of site-mixing, which affects their properties and was first quantified by Bragg and Williams with a long-range order parameter.[52] Over the years, numerous adaptations of the parameter have been developed, and they continue to serve an important role in various areas of materials chemistry.[53-55]. More recently, these analyses have been applied to semiconducting materials.[56] Here, to better quantity the ordering behavior in the mixed-chalcogen products, the following order parameter η was employed:

$$\eta = \frac{Q_{occ} - SS_{occ}}{1 - SS_{occ}}$$

where Q_{occ} is the observed occupancy at a given Q site and SS_{occ} is the expected occupancy at that site in a perfect a solid solution. Hence, for a fully ordered system η = 1, and for a fully disordered system η = 0 (solid solution). This order parameter does not offer the same utilities as those used to assess order-disorder phase transitions in metal alloys, but it does provide a useful metric for quantifying chalcogen ordering. Additionally, it can be used to assess the distinctiveness of each site within a given anion sublattice, as described below.

The refined occupancy and calculated ordering parameters for the three $CsCu_5Q_2Q'$ compounds are listed in Table S4. We note that the expected ratio of chalcogens in the solid solution (SS_{occ}) changes slightly across the series. This is due to marginal discrepancies between the nominal and refined composition of the products. Numerous crystals from each compound were structurally characterized, and deviations between nominal and refined compositions did not exceed

5%. Figure 3 shows the weighted average of the calculated order parameters (left axis) for the three $CsCu_5Q_2Q'$ compounds. Shannon-Prewitt radii for the divalent Q^{2-} chalcogen anions were used to calculate the percent difference in Q radii for each of the mixed-chalcogen permutations (right axis).[51] The experimentally determined ordering trends in the tetragonal $CsCu_5Q_2Q'$ track well with the relative size of the two chalcogens, where larger difference yields greater ordering. We note that although the tabulated ionic radii are for 6-coordinate chalcogen anions, the relative size of each anion within the same $P4_2/mnm$ structure is expected to follow the same trend.

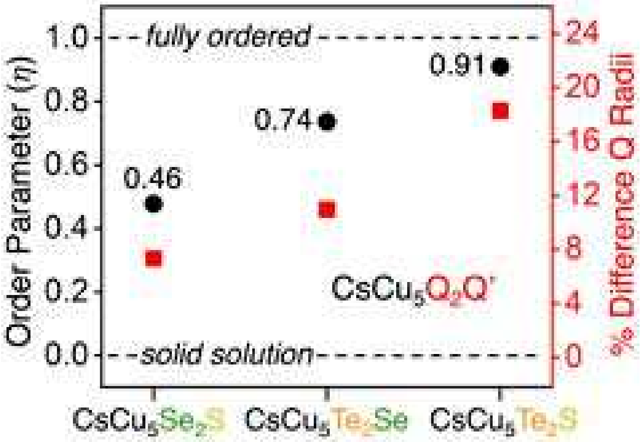

Figure 3. Weighted average of calculated order parameters for $CsCu_5Se_2S$, $CsCu_5Te_2Se$, and $CsCu_5Te_2S$. The percent difference of anionic radii from the corresponding Q/Q' chalcogens are plotted on the right (red) axis using tabulated Shannon-Prewitt values, where Q' represents the smaller chalcogen.

While detailed property analysis of the compounds is outside the scope of the study, the powder X-ray diffractograms (pXRD) of the bulk $CsCu_5Q_2Q'$ powders do not show any significant impurities. Panels A-C in Figure S1 show pXRD from finely ground ingots of $CsCu_5Se_2S$, $CsCu_5Te_2Se$, and $CsCu_5Te_2S$ products, along with simulated patterns from the corresponding SCXRD analysis. Visual inspection of the experimental and simulated patterns indicate good agreement with slight discrepancies in peak intensities, which is likely due to preferred orientation. Attempts to synthesize the $CsCu_5Te_3$ and $CsCu_5S_3$ end members through direct synthesis were unsuccessful, resulting in a mixture of phases that did not include the tetragonal $P4_2/mnm$ structure.

Chalcogen Ordering in Orthorhombic $BaCu_4Q_3$. To further explore how anion coordination influences chalcogen ordering, substitution experiments were performed on the $BaCu_4S_3$ structure. $BaCu_4S_3$ adopts the orthorhombic *Pnma* space group, and the structure is shown in Figure 4A.[57] This material is a p-type semiconductor with high band degeneracy and reported to exhibit good thermoelectric performance.[58] Similar to $CsCu_5Se_3$, it is composed of distorted trigonal CuS_3 and tetrahedral CuS_4 building blocks that assemble into an anionic framework with 1D channels, which are occupied by divalent Ba^{2+} cations.

The asymmetric unit of $BaCu_4S_3$ has one Ba atom, four Cu atoms, and three crystallographically distinct S atoms. The bonding environment for each chalcogen on the anion sublattice are shown in Figure S2. Here, S1 forms three bonds with Cu (3-coordinate), S2 forms five bonds with Cu (5-coordinate), and S3 forms six bonds with Cu (6-coordinate). The sulfur-metal interatomic distances in $BaCu_4S_3$ are shown in Table 2. From a bonding perspective, S1 is expected to be the most ionic site since it interacts with 3 Ba^{2+} cations and forms only three polar-covalent S-Cu bonds. The distinction between S2 and S3 is less clear since they coordinate with a similar number of Cu atoms (5- and 6-coordinate). Additionally, both anions interact ionically with two adjacent Ba^{2+} cations. Closer inspection of the Table 2 reveals the mean S-Cu bond length for S2 is 2.404 Å, and 2.484 Å for S3. The slightly higher coordination number and longer S-Cu bond distances suggest that S3 is more amenable to larger anions in mixed-chalcogen products.

BVS and Bader analyses were calculated for $BaCu_4S_3$ and the data listed in Table S1 and Table S2, respectively. The BVS value of S1 is determined to be 2.19, S2 is 2.10, and S3 is 1.79. Again, the sub-2 value for S3 indicates the anion at this site is underbonded, which may reflect the accessible volume at the Wyckoff position. The calculated Bader charge for Se1, Se2, and Se3 are found to be -0.92, -0.92, and -0.89, respectively. The lower charge at the Se3 site is in line with the other analyses, and suggests this would be the preferred crystallographic location of heavier, less electronegative chalcogens.

Although the $BaCu_4S_3$ structure provides a good comparison with $CsCu_5Se_3$, the sulfide host is found to be less amenable to chemical substitution. Indeed, attempts to substitute Te for S were unsuccessful and the solubility range for $BaCu_4S_{3-x}Se_x$ was limited to x values no greater than 2, since $BaCu_4Se_3$ adopts an alternate structure type. Nonetheless, analysis of the $BaCu_4S_2Se$ ($x = 1$) product proved insightful and exhibits trends that are consistent with other x values. $BaCu_4S_2Se$ was prepared by direct reaction of elemental precursors at high temperature. Briefly, stoichiometric amounts of Ba, Cu, S, and Se were loaded into carbon-coated quartz tubes and then flame-sealed under dynamic vacuum. The reaction vessels were heated to 1123 K in a box furnace, dwelled for 24 h, then radiatively cooled in the furnace. Black plate-like crystals suitable for SCXRD were isolated from the ingot product. Full details can be found in the experimental section.

Table 2. Selected Sulfur-Metal Interatomic Distances for $BaCu_4S_3$

atom pair	bond distance (Å)	atom pair	bond distance (Å)
S**1**–Cu3	2.2461(6)	S**2**–Cu4	2.7040(8)
S**1**–Cu1	2.2796(5) × 2	S**2**···Ba1	3.1543(7) × 2
S**1**···Ba1	3.1158(6) × 2	S**3**–Cu1	2.3425(9)
S**1**···Ba1	3.2762(9)	S**3**–Cu4	2.3713(7)
S**2**–Cu2	2.2849(6)	S**3**–Cu2	2.4353(5) × 2
S**2**–Cu4	2.3279(5) × 2	S**3**–Cu3	2.6608(5) × 2
S**2**–Cu3	2.3747(6)	S**3**···Ba1	3.3135(7) × 2
S**2**–Cu4	2.7040(8)		

$BaCu_4S_2Se$ crystallizes in the same the *Pnma* space group as the sulfide host structure and is shown in Figure 4B. Crystallographic tables and structural refinement details can be found in Table S3. The nominal ratio of chalcogens is 67% S and 33% Se, which is the expected occupancy at each Q site in a true solid solution. The refinement shows Q1 has an occupancy of 84% S and 16% Se (4C), with a calculated η value of 0.55. The S-rich Q1 site is expected considering it has the lowest coordination number and relatively short S-Cu bond distances in the host structure. Figure 4C shows the coordination environment at the Q2 site, which has a refined occupancy of 77% S (33% Se). This is slightly S-rich relative to the expected occupancy in a perfect solid solution, giving a η value of 0.36, which is the lowest value of the three sites. Conversely, Se shows a strong preference for the Q3 site (Figure 4D) with a refined occupancy of 68% Se and 32 % S, which gives a η value of 0.91. Here, the calculated order parameters offer some insight into the distinctiveness of the different positions on the anion sublattice of $BaCu_4S_3$.

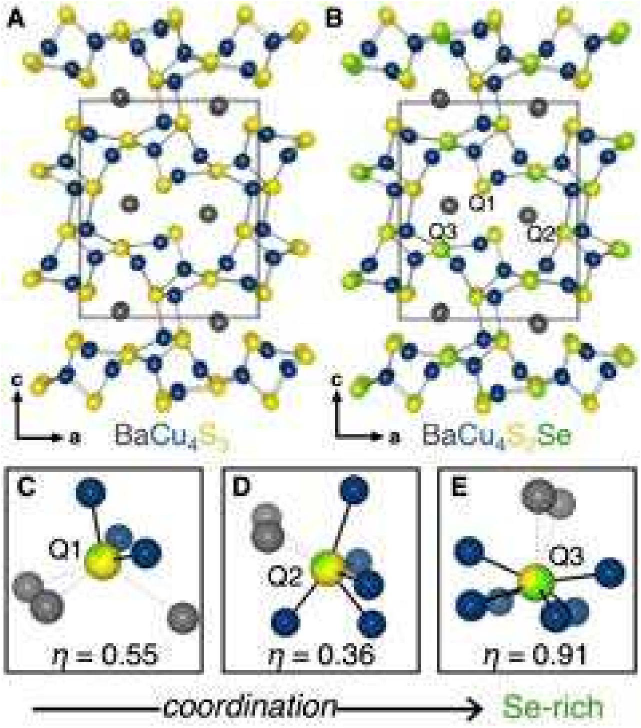

Figure 4. (A) Crystal structure of $BaCu_4S_2Se$ viewed along the b-axis, showing the 3D $[Cu_4Q_3]^{2-}$ framework with 1D pores occupied by counterbalancing Ba^{2+} cations. The coordination geometry for (B) Q1, (C) Q2, and (D) Q3 show increasing coordination correlates with greater Se occupancy. Calculated order parameters (η) are listed for each Q site, where the Q site with intermediate coordination (Q2) has occupancy closest to the overall anion composition. Ba atoms are colored in dark grey, Cu atoms in blue, S atoms in yellow, and Se atoms in green.

Although the $BaCu_4S_3$ structure provides a good comparison with $CsCu_5Se_3$, the sulfide host is found to be less amenable to chemical substitution. Indeed, attempts to substitute Te for S were unsuccessful and the solubility range for $BaCu_4S_{3-x}Se_x$ was limited to x values no greater than 2, since $BaCu_4Se_3$ adopts an alternate structure type. Nonetheless, analysis of the $BaCu_4S_2Se$ (x = 1) product proved insightful and exhibits trends that are consistent with other x values. $BaCu_4S_2Se$ was prepared by direct reaction of elemental precursors at high temperature. Briefly, stoichiometric amounts of Ba, Cu, S, and Se were loaded into carbon-coated quartz tubes and then flame-sealed under dynamic vacuum. The reaction vessels were heated to 1123 K in a box furnace, dwelled for 24 h, then radiatively cooled in the furnace. Black plate-like crystals suitable for SCXRD were isolated from the ingot product. Full details can be found in the experimental section.

$BaCu_4S_2Se$ crystallizes in the same the *Pnma* space group as the sulfide host structure and is shown in Figure 4B. Crystallographic tables and structural refinement details can be found in Table S3. The nominal ratio of chalcogens is 67% S

and 33% Se, which is the expected occupancy at each Q site in a true solid solution. The refinement shows Q1 has an occupancy of 84% S and 16% Se (4C), with a calculated η value of 0.55. The S-rich Q1 site is expected considering it has the lowest coordination number and relatively short S-Cu bond distances in the host structure. Figure 4C shows the coordination environment at the Q2 site, which has a refined occupancy of 77% S (33% Se). This is slightly S-rich relative to the expected occupancy in a perfect solid solution, giving a η value of 0.36, which is the lowest value of the three sites. Conversely, Se shows a strong preference for the Q3 site (Figure 4D) with a refined occupancy of 68% Se and 32 % S, which gives a η value of 0.91. Here, the calculated order parameters offer some insight into the distinctiveness of the different positions on the anion sublattice of $BaCu_4S_3$.

The refined composition for the $BaCu_4S_2Se$ crystals deviated slightly from the nominal composition, but were within 5% of the expected values. Again, this implies a slight variation in the composition of crystallites within the bulk product, which could be due to incongruent melting. However, the pXRD of the ground $BaCu_4S_2Se$ ingot matches well with the simulated pattern (Figure S3), without any significant impurities.

Chalcogen Ordering in Layered $NaCuZrQ_3$. The ternary host structures described above contain only one type of Q-metal bond. In such systems, the anion coordination number and bond distances found in the parent structures prove to be good descriptors for predicting ordering behavior. However, host structures with chalcogen anions that form covalent bonds with multiple, distinct metal centers, the strength of the Q-metal bonds must be considered. To explore the importance of bond enthalpy in chalcogen ordering, we performed chalcogen substitutions on the layered $NaCuZrSe_3$ quaternary host structure. The crystallographically distinct Se anions in this structure form bonds with both soft, monovalent Cu^+ cations and relatively hard, tetravalent Zr^{4+} metal centers. Each Se anion in the host has a different ratio of Se-Cu to Se-Zr bonds. Accordingly, $NaCuZrSe_3$ was chosen as a suitable system to demonstrate the utility of hard-soft acid-base (HSAB) bonding concepts when predicting anion segregation in these types of compounds.

Although the sulfoselenide and sulfotelluride $NaCuZrQ_{3-x}Q_x$ products described in this section can be made directly through high-temperature solid-state methods, the resulting products did not yield crystals suitable for SCXRD. Accordingly, needle-like $NaCuZrQ_{3-x}Q'$ crystals were first synthesized by reacting stoichiometric amounts of elemental precursors in a NaCl flux, which were found to be suitable for structural analysis. Full details regarding both syntheses can be found in the Experimental Section. Crystallographic data tables and information regarding structural refinements can be found in Table S6.

$NaCuZrSe_3$ has a layered structure with the *Pnma* space group and is shown in Figure 5A.[59] The structure can be described as layers of anionic $[CuZrSe_3]^-$ slabs that are counterbalanced by Na^+ cations. The material belongs to the AMM'Q_3 class of compounds, a diverse family of layered materials with several related structure types. Ibers and coworkers categorized these compounds into sub-types according to the oxidation state of the A, M, and M' metal cations.[19] According to this classification, $NaCuZrSe_3$ is a member of the type-I subclass, where the atoms have formal oxidation states of $A^{+1}M^{+1}M^{+4}(Q^{2-})_3$.

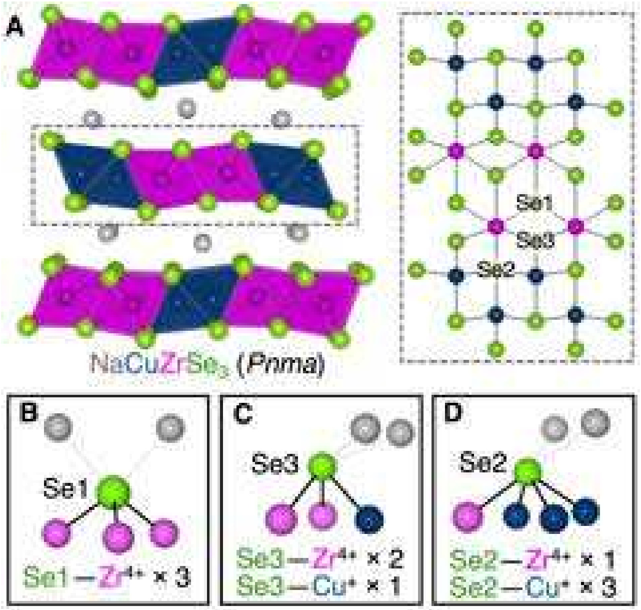

Figure 5. (A) Crystal structure of $NaCuZrSe_3$ viewed along the b-axis showing layers composed of $CuSe_4$ tetrahedra and $ZrSe_6$ octahedra separated by Na^+ cations. The single [CuZrSe3] layer viewed along the a-axis is illustrates the distinct coordination of each Se anion. Isolated coordination spheres for (B) Se1, (C) Se3, and (D) Se2 have varying number of Se-Zr and Se-Cu bonds.

The two-dimensional slabs in the *Pnma* structural variant are composed of edge-sharing $ZrSe_6$ octahedra (O) and $CuSe_4$ tetrahedral (T) building blocks that are connected in a repeating OOTT sequence. The asymmetric unit for $NaCuZrSe_3$ has one Na, Cu, and Zr atom, along with three crystallographically distinct Se atoms. On the right side of the panel in Figure 5A the $[CuZrSe_3]$ slab is viewed along the b-axis, highlighting the differing coordination environment at the three Se sites. Panels B-D in Figure 5 show the isolated coordination spheres for the three sites viewed from the b-axis. Here, Se1 coordinates to three Zr atoms, Se3 coordinates to two Cu and one Zr atom, while Se2 forms one bond with Zr and three bonds with Cu. The Se-metal interatomic distances are shown in Table S7. Intuitively, the Se1 site is the most distinct of the three Se atoms since it coordinates exclusively to the Zr^{4+} metal centers. Accordingly, the substitutional studies targeted sulfoselenide and sulfotelluride products with a nominal composition of $NaCuZrQ_2Q'$, where Q' represents the smaller, more electronegative chalcogen. The selenotelluride analogues were successfully synthesized according to pXRD, but the products from the flux synthesis did not yield crystals that were suitable for SCXRD analysis.

BVS and Bader analyses were used to augment the qualitative assessments described above, and the data are tabulated in Table S1 and Table S2. The three unique Se anions have BVS near 2, with Se1 at 2.17, Se2 at 1.83, and Se3 at 1.96. Again, the BVS values appear to be correlated with the calculated Bader charges, where Se1, Se2, and Se3 are determined to be -1.10, -0.82, and -0.96.

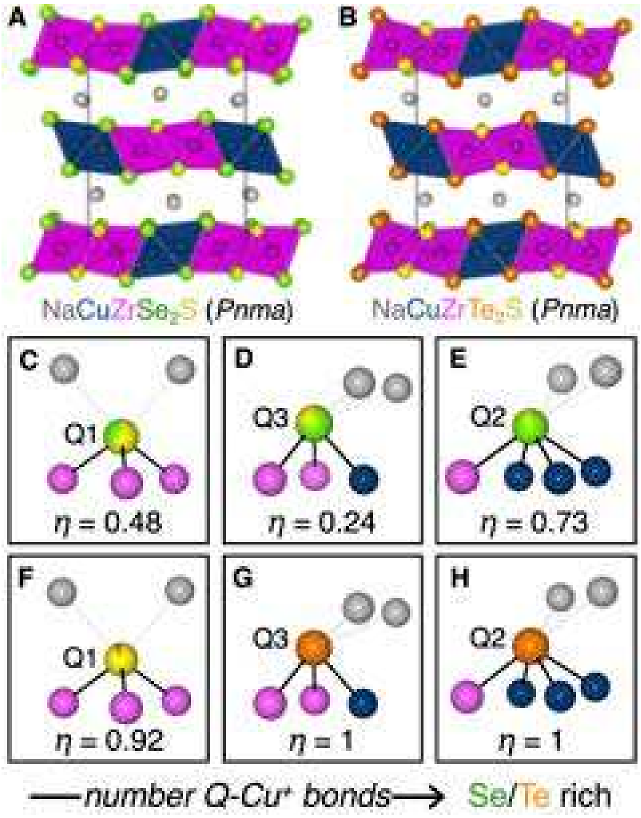

Figure 6. Crystal structure of (A) $NaCuZrSe_2S$ and (B) $NaCuZrTe_2S$ viewed along the b-axis. Anion bonding environments for Q sites in $CsCu_5Se_2S$ (C-E) and $CsCu_5Te_2S$ (F-H), where pie charts depict occupancy. Calculated order parameters for each site (η) indicate Q1 and Q2 are most distinct, prefer harder (S) and softer (Se, Te) chalcogens, respectively.

$NaCuZrSe_2S$ (Figure 6A) and $NaCuZrTe_2S$ (Figure 6B) are both found to crystallize in the same layered *Pnma* structure as the selenide host. Again, the nominal stoichiometry is 67% Q and 33% Q', which also represents the expected occupancy at each site on the anion sublattice in a true solid solution. The bonding environment of the three Q sites in the $NaCuZrSe_2S$ product are shown in panels C through E in Figure 6. The refined occupancy for Q1 is 65% S (35% Se), which is S-rich relative to the overall composition and gives a calculated η value of 0.48. The Q3 site, which forms two bonds with Zr and one bond with Cu, is found to be 75% Se (25% S), which is closest to the overall composition and accordingly, the lowest degree of ordering (η = 0.24). The Q2 occupancy is determined to be 91% Se (9% S), which is Se-rich and gives this site a η value of 0.73. Similar to the ternary $CsCu_5Q_3$ system, the sulfotelluride product shows the greatest degree of ordering. Panels F through H in Figure 6 show the coordination environment for the three distinct Q sites in the $NaCuZrTe_2S$ product. The structural refinement indicates Q1 occupancy of 92% S (8% Te), while the Q2 and Q3 sites are 100% Te. We note that the overall stoichiometry for the $NaCuZrTe_2S$ product deviates slightly from the nominal reaction composition. Numerous crystals were characterized with SCXRD, some of which were closer to the nominal composition but with inferior refinement statistics. Accordingly, we have reported the data with the superior structural refinement.

The data from the mixed-chalcogen products clearly indicate that the larger, more polarizable chalcogen anions show a strong preference for the Q2 and Q3 sites, where they are able to form favorable soft-soft acid-base interactions. Additionally, the S^{2-} anions show a strong preference for the Q1 site, with η values of 0.48 and 0.92 in the sulfoselenide and sulfotelluride products, respectively. Again, the preferential occupancy is attributed to bonding factors, where the relatively hard S^{2-} anions occupy positions where they coordinate exclusively to the harder Zr^{4+} cations. Meanwhile, the larger, more polarizable chalcogen shows a strong preference to occupy the Q2 site, where they form three favorable $Te^{2-}(Se^{2-})$-Cu^{+} interactions. In the sulfoselenide, because the sulfur segregates to the Q1 site and Se to the Q2 site, the Q3 site has a composition that is closest to the hypothetical solid solution. Accordingly, this site has the lowest η value in the series (0.25). The $NaCuZrTe_2S$ product is ostensibly fully ordered, with Te fully occupying the Q2 and Q3 sites. Sulfur is found exclusively at the Q1 site, where the refined occupancy was determined to be 92% S and 8% Te, indicating an 8% deviation from the nominal reaction composition. Clearly, the presence of multiple metal centers changes the calculus when predicting how chalcogens will be distributed in a host lattice.

As for all of the compounds reported, several syntheses were performed, and numerous crystals were analyzed. The 8% deviation between the nominal and refined stoichiometry of the $NaCuZrTe_2S$ product represents the upper limit observed in this system. It is included in the report due to higher quality SCXRD data and better corresponding structural refinement. It is likely that the average crystallite in the product is closer to the nominal composition. The pXRD patterns for $NaCuZrSe_2S$ and $NaCuZrTe_2S$ bulk powders are shown in panels A and B of Figure S4, respectively. The diffractogram for the sulfoselenide sample displays significant preferred orientation, which is commonly observed in materials with 2D structures. The sulfotelluride pattern displays less preferred orientation, with peaks consistent with the simulated pattern and no significant impurities.

Chalcogen Ordering in Quaternary $Ba_2BiFeSe_5$. To expand the scope of the study, and further understand the role that Q-metal bonding plays in ordering phenomena, we employed a substitutional study on the $Ba_2BiFeSe_5$ quaternary system. The compound, as well as the sulfide analogue, have been reported to exhibit antiferromagnetic behavior.[60, 61] The structure is shown in Figure 7A and is composed of distorted $BiSe_6$ octahedra and $FeSe_4$ tetrahedra. The $BiSe_6$ units share edges with each other to form chains along the b-axis, which are linked covalently by $FeSe_4$ tetrahedra to form corrugated 1D channels that are occupied by Ba^{2+}. The asymmetric unit has one Ba, Bi, and Fe atom, and four distinct Se atoms. An interesting structural feature is that each polyhedral building block has a Se anion that is not fully coordinated, essentially in a dangling position along the corrugated pores (Figure 7B and 7C). Specifically, Se2 forms one covalent bond to Bi^{3+} (relatively soft acid), and four ionic interactions with Ba^{2+} with an average distance of 3.3815(8) Å. Likewise Se4 forms one covalent bond to Fe^{3+} (relatively hard acid), and four ionic interactions with Ba^{2+} with an average distance of 3.396 Å. Hence, the Se2 and Se4 sites are essentially identical except for the nature of the trivalent metal they are bound to.

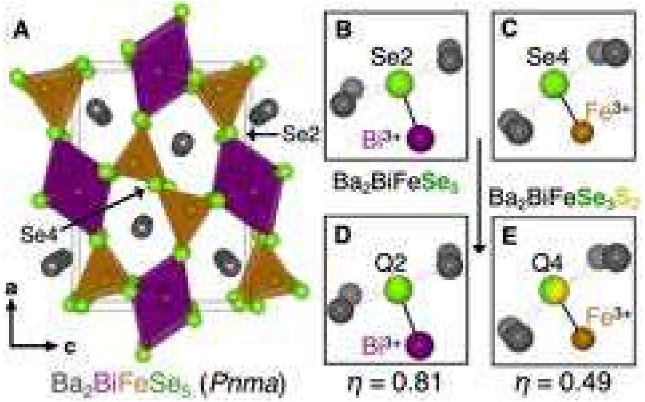

Figure 7. (A) Crystal structure of orthorhombic $Ba_2BiFeSe_5$ viewed along the b-axis, showing $FeSe_4$ tetrahedra that act as linkers between chains of edge-sharing $BiSe_6$ octahedra. Bonding environment for (B) Se2 and (C) Se4 anions, which have similar coordination geometry but are bonded to different trivalent metals. Refined occupancy at the (D) Q2 and (E) Q4 site in $Ba_2BiFeSe_3S_2$ are found to be Se-rich and S-rich, respectively, relative to overall composition.

$Ba_2BiFeS_2Se_3$ crystallizes in the same orthorhombic structure as the single-anion end members. Crystallographic and refinement details can be found in Tables S8, and the anion composition from the refined structure was determined to be 38% S and 62% Se. The Q1 and Q3 sites show the least degree of ordering, with η values of 0.02 and 0.28, respectively. The coordination geometry for the Q2 and Q4 sites are shown in panels D and E of Figure 7, respectively. Clearly, the Se anions shows strongest preference for the Q2 site with a η value of 0.82. This is attributed to favorable soft-soft acid-base interaction between the relatively large Se^{2-} and soft Bi^{3+} metal. Conversely, the Q4 site is 57% S, much higher than the expected value for a solid solution, with a calculated η value of 0.49. Again, hard-soft acid-base principles provide rationale for the ordering, where the harder, more electronegative S^{2-} anions prefers sites where they can form bonds with the relatively hard Fe^{3+} metals. This substitutional study is insightful, where ordering at the Q2 and Q4 sites can be attributed explicitly to favorable bonding interactions, since it is decoupled from other variables such coordination geometry and oxidation state.

The pXRD for the $Ba_2BiFeS_2Se_3$ is shown in Figure S5 along with the simulated pattern from the SCXRD analysis. The peaks in the experimental diffractogram match well

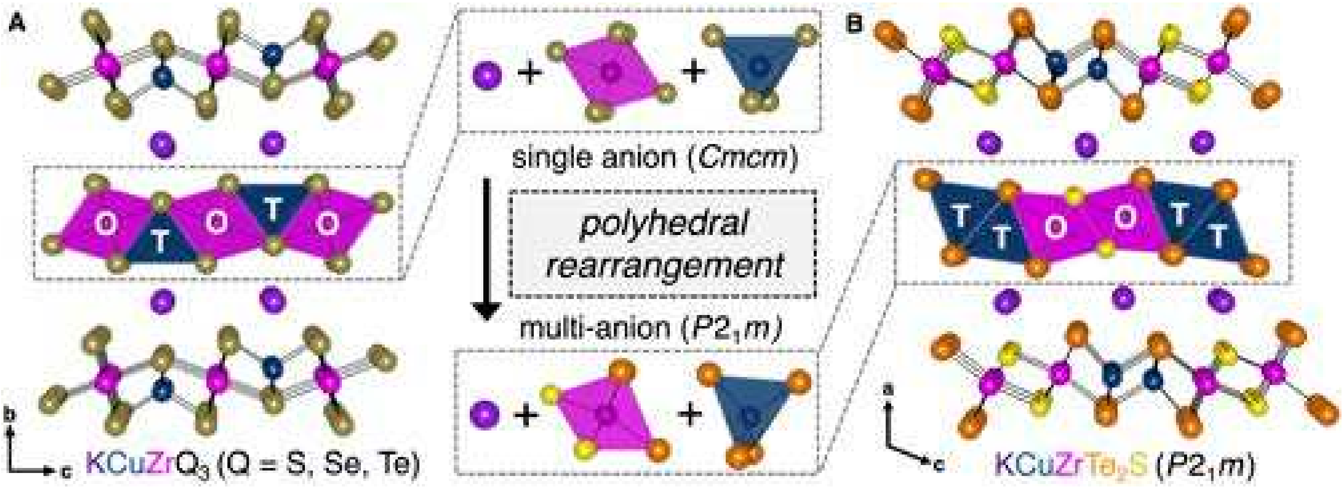

Figure 8. (A) Crystal structure of orthorhombic $KCuZrQ_3$ viewed along the a-axis, which is adopted by all three single-chalcogen compounds. The center layer is shown with the polyhedral depiction, illustrating the OTOT repeating sequence of ZrQ_6 (O) octahedra and CuQ_4 (T) tetrahedra. (B) Structure of monoclinic $KCuZrTe_2S$ viewed along the b-axis. The polyhedra depiction of the center slab illustrates the alternate OOTT sequence of polyhedral building blocks.

with the simulated pattern, with the exception of the peak at 26 degrees, which has unexpectedly high intensity. This could be due to enhanced intensity from the (022) peak due to preferred orientation. The only other peak in the experimental that is unaccounted for is at 57 degrees, which is the location of the (044) peak, which is parallel to (022). Alternatively, this could be from an unidentified impurity. Since property measurements were not the focus of this study, no additional optimization or characterization was pursued.

Polyhedral Rearrangement in Layered $KCuZrTe_2S$. In systems where multiple polymorphs share similar energy, we find that mixed-chalcogen products can adopt structures not found in their single-anion end members. Here, we illustrate this concept with a substitutional experiment on the layered $KCuZrQ_3$ parent structure.

The $KCuZrTe_2S$ compound was discovered while performing substitution experiments on single-anion AMM'Q_3 compounds with the *Cmcm* structural variant. All three single-anion $KCuZrQ_3$ quaternaries have been reported previously and adopt the same 2D structure with the *Cmcm* space group,[62] which is shown in Figure 8A. Like $NaCuZrSe_3$, the potassium analogues belongs to the type-I subclass of the AMM'Q_3 family of compounds. These systems can have one of several related structure types, which are differentiated by the arrangement of tetrahedral and octahedral building blocks. In the *Cmcm* phase, anionic $[CuZrQ_3]^-$ slabs composed of edge-sharing CuQ_4 tetrahedra and ZrQ_6 octahedra are separated by layers of counterbalancing K^+ cations. When viewed along the a-axis, it can be seen that the tetrahedral (T) and octahedral (O) building blocks have a repeating OTOT sequence. The asymmetric unit for $KCuZrQ_3$ has one K, Cu, and Zr atom, and two unique Q atoms. Here, the Q1 anions form one bond with Cu and two bonds with Zr, while Q2 forms two bonds with Cu and two bonds with Zr. The local chemistry at the Q sites in the *Cmcm* structure are not as distinct as the *Pnma* phase, which have three unique Q sites that span a wider range of Q-Zr and Q-Cu bonds.

In order to evaluate chalcogen ordering in $KCuZrQ_3$, which have two Q sites with similar bonding, we targeted sulfotelluride products since they tend to have the highest degree of ordering. Needle-like crystals of $KCuZrTe_2S$ were first grown KCl flux and characterized using SCXRD analysis. Crystallographic information and refinement details can be found in Table S9, and full synthetic protocol for the reaction is described in the Experimental Section. The $KCuZrTe_2S$ product crystallizes in the $P2_1m$ space group, and the structure is shown in Figure 8B. This is a less common structural variant found in the AMM'Q_3 systems, and can be considered a distorted version of the *Pnma* structure. Here, the CuQ_4 tetrahedra and ZrQ_6 octahedra in the $[CuZrQ_3]^-$ slabs have an alternating OOTT arrangement, with three distinct Q sites similar to those shown in panels B-D in Figure 5 (*Pnma* $NaCuZrSe_3$). The polyhedral arrangement in the $P2_1m$ structure, which is distinct from the single-chalcogen analogues, enables S^{2-} and Te^{2-} anions to segregate onto sites where they can maximize the number of energetically favorable bonds. The rationale for the ordering is the same as described above for the $NaCuZrQ_3$ compounds with the *Pnma* structure. The refined structural data indicates the composition at the Q1 site is 81% S (19% Te), while Q2 and Q3 are found to be fully occupied by Te. We note that the discrepancy between the refined and nominal composition for this system is higher than the other reported compounds. Several crystals were analyzed, consistently showing refined compositions that were S-deficient. This could be due to differing solubility of Te and S precursors in the KCl flux, or alternatively, represent a solubility limit of S in the $P2_1m$ sulfotelluride.

DISCUSSION

A common trend across all of the studied systems is the relationship between the degree of ordering and the relative size of the two chalcogen radii. We conducted total energy calculations using DFT in an attempt to predict the degree of ordering in the mixed-chalcogen products. Modeling structures with mixed occupancy using DFT is notoriously challenging. One approach is to construct a supercell containing multiple unit cells with randomly distributed atoms. However, supercell calculations are computationally demanding, especially for large and complex systems.

Here, we introduce an alternative approach for modeling disorder that proves to be an effective, semi-quantitative tool for predicting ordering trends. The $CsCu_5Se_2S$ compound is used to illustrate the process. In the primitive cell of the $CsCu_5Se_2S$ compound, consisting of four formula units, there are 12 chalcogen anions with 8 sites occupied by Se anions and the remaining 4 sites occupied by S anions, assuming a fully ordered system. To mimic disorder, we introduced variations by switching Se and S sites within ordered configurations. Although there are 495 possible configurations (12 choose 4), considering symmetrically equivalent arrangements, we identified 72 distinct structures and computed their total energies (Figure S6). Among these structures, we set the most stable ordered configuration as the reference structure, where all Q1 sites are occupied by S anions and all Q2 sites are occupied by Se anions. We then calculated the difference in energy between the reference structure and alternative configurations.

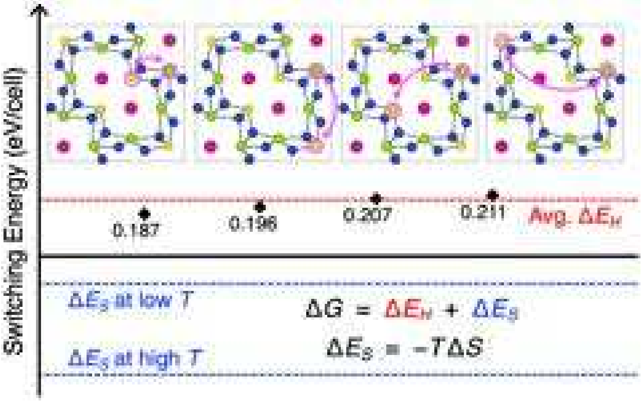

Figure 9. Illustration of switching energies (eV/primitive cell) for the $CsCu_5Se_2S$ compound when one pair of Se-S anion sites were switched. The primitive cell consists of four formula units. The reference structure, representing the most stable ordered configuration, is the fully ordered structure. The switched anions are marked with magenta arrows in the four configurations.

We observed that switching Se and S anions sites led to an increase in total energy. As shown in Figure S6, switching one, two, three, and four pairs of Se-S anions in the $CsCu_5Se_2S$ resulted in total energy increases of approximately 0.2, 0.38, 0.55, and 0.70 eV/primitive cell, respectively, compared to the most stable configuration. This indicates that total energy increases further as more chalcogen anions sites are switched, indicating a statistical preference for single pair switching rather than multiple pairs. In this study, we define switching energy as the total energy difference between the most stable configuration and the average of the single pair switching configurations. Higher switching energy represents a stronger tendency for Se and S anions to retain their original sites (Se anions tending to occupy Q2 sites, while S anions preferring Q1 sites). It leads to a higher degree of ordering within the system. Figure 9 illustrates the switching energies of $CsCu_5Se_2S$ when one pair of Se-S anion sites were switched. There are 4 possible configurations with one pair of switching, and the averaged value of the total energy change (i.e. switching energy) was determined to be 0.20 eV/primitive cell.

While our calculations only considered enthalpy in the DFT calculations, disregarding entropy contributions, it's important to note that Gibbs free energy, used to determine structure stability, has both enthalpy and entropy terms. Depending on temperature and entropy contributions, some alternative configurations may become more stable than the reference structure, resulting in a disordered system. By calculating averaged switching energies of mixed-chalcogen $CsCu_5Q_2Q'$ compounds and comparing them, we semi-quantified the ordering trends.

In Figure 10, the primary y-axis shows the average switching energy calculated of the mixed-anion $CsCu_5Q_3$ compounds using DFT (eV), and the secondary y-axis shows the corresponding ordering parameter (η). The averaged switching energies of $CsCu_5Se_2S$, $CsCu_5Te_2Se$, and $CsCu_5Te_2S$ were found to be 0.20, 0.25, 0.51 eV per primitive cell, respectively. The calculations correlate well with the experimental data, showing that $CsCu_5Te_2S$ the exhibits the highest degree of ordering while $CsCu_5Se_2S$ shows the lowest degree of ordering.

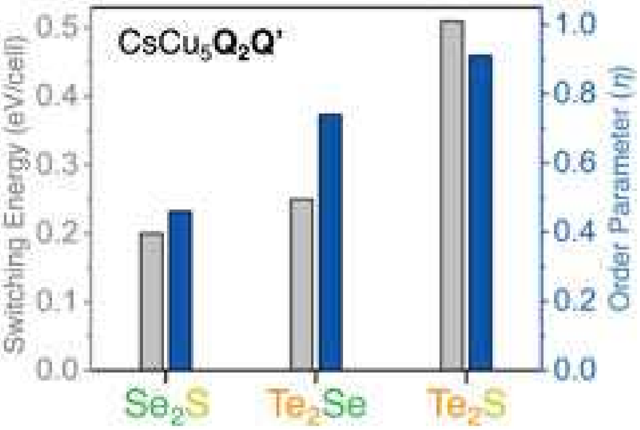

Figure 10. Histograms showing the calculated switching energy (eV/cell) for the $CsCu_5Q_2Q'$ compounds, which are plotted on the primary y-axis (left). Here, Q' represents the lighter of the two chalcogens. The weighted average of the calculated order parameter (η) for the corresponding compounds is shown on the secondary y-axis (right).

Additionally, we performed switching energy calculations for mixed-chalcogen $NaCuZrQ_2Q'$ compounds. The primitive cell of these compounds consists of four formula units, with 8 anion sites occupied by Q anions and the remaining 4 sites occupied by Q' anions in an ordered system. Since multiple pairs of anion switching are much less favorable than single pair switching, we computed the switching energies for $NaCuZrTe_2S$ and $NaCuZrSe_2S$ by considering one pair of switching and averaging the switching energies. The averaged switching energies for $NaCuZrTe_2S$ and $NaCuZrSe_2S$ were found to be 0.49 and 0.13 eV per primitive cell, respectively. Figure S7 illustrates these averaged switching energies, showing that $NaCuZrTe_2S$ exhibits the highest switching energy, while $NaCuZrSe_2S$ displays the lowest among the compounds. This ordering of switching energies suggests that $NaCuZrTe_2S$ has the highest degree of ordering, with the larger chalcogen Te preferring to occupy the Q2 and Q3 sites, while the smaller chalcogen S tends to occupy the Q1 sites. Conversely, the switching energy of $NaCuZrSe_2S$ demonstrates the lowest degree of ordering. These findings are in good agreement with experimental data, which revealed that in $NaCuZrTe_2S$, the Q2 and Q3 sites are fully occupied by Te, and the Q1 sites are 92% occupied by S. Similarly, the observed lower switching energy for $NaCuZrSe_2S$ aligns well with experimental results, where the Q2 and Q3 sites are occupied by Se with 91% and 75% occupancy, respectively, while the Q1 sites are occupied by S with 65% occupancy.

CONCLUSION

Multi-anion materials contain metal centers with distinct coordination geometries that offer chemists additional levers for tuning properties. While mixtures of isovalent anions tend to form solid solutions in simple crystal systems, ordering does occur in structures that have more than one crystallographically distinct anion site. In this report, we present rules and guidelines for predicting when and how anion ordering will occur in mixed-chalcogen materials. The ordering is attributed to the varying size and bonding affinity across the chalcogen series, and the degree of ordering depends on the distinctiveness of the chemistry at the anion sites, and additionally, the ratio of chalcogen radii in the product. Sulfotelluride products exhibit the largest degree of ordering, and additionally, these products can adopt structure types not found in the single-anion analogues. Here, rearrangement of polyhedral units enable stronger bonding interactions between the chalcogen anions and constituent metals.

From a synthetic perspective, the analysis provides a powerful framework for reverse-engineering solids with predetermined arrangements of anions and targeted bonding features. The strategy exploits the wealth of single-anion structures in the structural databases, providing an endless library of substrates for exploring multi-anion phenomena. Although the proof-of-principle study focuses on metal chalcogenides, we believe the technique will prove applicable to a variety of other material systems and accelerate exploratory efforts.

EXPERIMENTAL

Starting Materials and Synthetic Protocol. All manipulations were performed in a N_2-filled glovebox. Bismuth chunks (Bi, 99.9%), copper chunks (Cu, 99.999%), selenium shot (Se, 99.999%), sulfur flakes (S, 99.999%), and tellurium shot (Te, 99.999%) were purchased from American Elements. Sodium chunks (Na, 98%) were purchased from Fisher Scientific. Cesium metal (Cs, 99.8%) was purchased from Thermo Scientific. Barium sulfide (BaS, 99.9%), iron chips (Fe, 99.98%), zirconium chunks (Zr, 99%), and sodium chloride (NaCl, 99%) was purchased from Sigma-Aldrich. Prior to use, sodium chloride was placed in a vacuum oven for 24 h at 523 K to remove residual water.

Synthesis of Binary Alkali Chalcogenides. Cs_2Q (Q = S, Se, Te) binary precursors were prepared by reacting Cs metal with the respective chalcogen in liquid ammonia, as previously described. Approximately 20 g of the targeted binary chalcogenide was prepared in each reaction. A 5% excess of chalcogen was employed to prevent the presence of unreacted metal in the final product. Moreover, grinding the chalcogen precursor into a fine powder helps reduce the reaction time and improves the homogeneity of the product. The dried binary chalcogenides were stored in the N_2-filled glovebox for further use.

Synthesis of Mixed-Chalcogen $CsCu_5Q_{3-x}Q'$ Compounds. The $CsCu_5Se_3$, $CsCu_5Se_2S$, $CsCu_5Te_2Se$, and $CsCu_5Te_2S$ compounds were prepared using high-temperature solid-state reactions of stoichiometric amounts Cs_2Q, Cu, and additional respective chalcogens aiming for a total mass of 1 g. Keeping the copper in exact stoichiometric amount is important to avoid the formation of $CsCu_4Q_3$ phase. Precursors were loaded into a carbon-coated fused silica tubes with 10 mm inner diameter, and then flame-sealed under dynamic vacuum (10^{-3} Torr). The sealed reaction vessels were placed in a programmable box furnace and heated to 723 K at a rate of 100 K/h. The vessels were annealed at that temperature for 10 h to allow partial reaction of the chalcogen precursors. The temperature was then ramped to 1123K at 100 K/h, and soaked for 6 hours. The furnace was then turned off and cooled to room temperature by radiative cooling. The ampules were then cracked open in air, revealing homogenous ingot products. The ingot was broken into pieces and black plate-like crystals were hand-picked under an optical microscope for single-crystal X-ray diffraction characterization. The ingot was then pulverized into a fine powder using a mortar and pestle for subsequent powder X-ray diffraction characterization.

Synthesis of $BaCu_4SeS_2$. Stoichiometric amounts of elemental precursors (Ba, Cu, Se, S) were loaded into a carbon-coated fused silica tube with 10 mm inner diameter, and then flame-sealed under dynamic vacuum (10^{-3} Torr). The reaction vessel was placed in a programmable box furnace, ramped to 723 K at a rate of 100 K/h and then annealed for 5 h. The furnace was heated to 1123 K at the same rate, soaked for 5 h, then radiatively cooled to room temperature.

Synthesis of Mixed-Chalcogen $NaCuZrQ_2Q'$ compounds. $NaCuZrSe_2S$ and $NaCuZrTe_2S$ were first synthesized in a NaCl flux to produce crystal suitable for SCXRD. Stoichiometric amounts of Na, Cu, Zr, and targeted chalcogens (S, Se, Te) equaling 1 g was place into a carbon-coated fused silica tube in a N_2-filled glovebox. 2 g of dry NaCl was then loaded on top of the precursors, and the tubes were sealed under dynamic vacuum (10^{-3} Torr). The tubes were then placed in a programmable box furnace and ramped to 723 K at 100 K/h. After soaking at that temperature for 10 h, the furnace was heated to 1273K for complete melt of the NaCl flux, and soaked at that temperature for 24 hours. The reaction was then cooled to 873K at a rate of 10 K/h, and then the furnace was then turned off and the samples radiatively cooled to room temperature. The reaction ampules were broken in air, and the needle like crystals were isolated using an optical microscope for subsequent SCXRD characterization. Bulk powders of the samples were prepared using high-temperature solid-state reaction of reaction the elemental precursors. In brief, stoichiometric amounts of elemental precursors were placed in carbon-coated fused silica tubes, sealed under dynamic vacuum, and then heated using the same temperature profile as the flux synthesis. The resulting product was a homogeneous-looking lump, which was pulverized with a mortar and pestle for subsequent characterization using powder X-ray diffraction.

Synthesis of $Ba_2BiFeSe_3S_2$. Stoichiometric amounts of elemental precursors (Ba, Fe, Bi, Se, S) were loaded into a carbon-coated fused silica tube with 10 mm inner diameter, and then flame-sealed under dynamic vacuum (10^{-3} Torr). The reaction vessel was placed in a programmable box furnace, ramped to 723 K at a rate of 100 K/h and then annealed for 5 h. The furnace was heated to 1073 K at the 100 K/h, annealed for 96 h, then radiatively cooled to room temperature.

Single-Crystal X-ray diffraction. Suitable single crystals were were coated with Paratone oil, mounted on a Nylon loop, and transferred to a ROD, Synergy Custom system, HyPix-Arc 150 diffractometer at 40 kV and 30 mA. Frames were collected at 173K. The radiation source was Cu Kα radiation (λ=1.5406 Å) for all samples. Space-group assignments were based on systematic absences, normalized structure factor statistics (*E* statistics), agreement factors for equivalent reflections, and successful refinement of the structure. The structures were solved by direct methods, expanded through successive difference Fourier maps using SHELXT, and refined against all data using the SHELXL-2014 software package as implemented in Olex2. Weighted *R* factors, R_w, and all goodness-of-fit indicators are based on F^2. Summary diffraction and refinement statistics can be found in the Supplementary Tables.

Powder X-ray Diffraction. For powder X-ray diffraction characterization, ingot products were pulverized into a fine powder using an agate mortar and pestle. The phase purity of the resulting bulk powder was then analyzed using a benchtop Bruker D2 PHASER diffractometer with Cu Kα radiation (λ = 1.5406 Å).

Density Functional Theory Calculations. In this study, density functional theory (DFT) calculations[63] were conducted using the Vienna Ab-initio Simulation Package (VASP)[64-66] with the projector-augmented wave (PAW)[67] method and plane-wave basis sets. Since it is challenging to directly calculate disordered systems, we calculated switching energies to verify the anion ordering trends of $CsCu_5Q_3$ and $NaCuZrQ_3$ compounds. Here, we define the switching energy as a total free energy difference between the most stable ordered structure and alternate configurations resulting from anion site exchanges (S-Te, Se-Te, and S-Se). For the total energy calculations, structure relaxation was performed using the revised Perdew-Burke-Ernzerhof for solids (PBEsol) of the generalized gradient approximation (GGA)[68] exchange-correlation functional. A plane-wave cutoff energy of 520 eV was used, and the k-points were evenly sampled with a k-spacing parameter of 0.25. Convergence of cutoff energy and k-spacing were checked, ensuring reliability. The energy and force convergence thresholds were set to 10^{-5} eV and 10^{-2} eV/Å, respectively.

ASSOCIATED CONTENT

Supporting Information

The Supporting Information is available free of charge on the ACS Publications website.

Crystallographic data files for the structures in this paper are available by request to the Cambridge Crystallographic Data Centre (CCDC) in the form of crystallographic information files with associated CCDC numbers of 2306656 ($CsCu_5Se_2S$), 2306652 ($CsCu_5Te_2Se$), 2306653 ($CsCu_5Te_2Se$), 2371320 ($BaCu_4S_2Se$), 2307663 ($NaCuZrSe_2S$), 2307662 ($NaCuZrTe_2S$), and 2371360 ($Ba_2BiFeSe_3S_2$). These data can be obtained free of charge from CCDC (https://www.ccdc.cam.ac.uk/); pXRD, and full crystallographic tables for all of the reported compounds (PDF)

AUTHOR INFORMATION

Corresponding Author

* **James M. Hodges** – Department of Chemistry, Pennsylvania State university, University Park, Pennsylvania 16802, United States; orcid.org/0000-0002-2306-0845
Email: hodges@psu.edu

Author Contributions

The manuscript was written through contributions of all authors. All authors have given approval to the final version of the manuscript.

Notes

The authors declare no competing financial interest.

ACKNOWLEDGMENT

This work was supported in part by the Eberly College of Science and the Department of Chemistry at the Pennsylvania State University. Characterization was conducted at the Integrated Macromolecular and Small Molecule X-ray Crystallography Facility, and the Materials Characterization Lab, both at Penn State. The authors thank Hemant Yennawar for assistance with structural characterization and acknowledge support from National Institutes of Health through Awards #1S10OD028589-01 and #1S10RR023439-01 for X-ray instrumentation. H.L. and Y.X. acknowledge support from the US National Science Foundation through Award 2317008 (phonon calculations). The authors acknowledge the comput- ing resources provided by Bridges2 at the Pittsburgh Supercomputing Center (PSC) through Allocations mat220006p and mat220008p from the Advanced Cyber- infrastructure Coordination Ecosystem: Services & Support (ACCESS) program, which is supported by National Science Foundation Grants 2138259, 2138286, 2138307, 2137603, and 2138296.

REFERENCES

(1) Canfield, P. C.; Fisher, I. R. High-temperature solution growth of intermetallic single crystals and quasicrystals. *Journal of Crystal Growth* **2001**, *225* (2), 155-161.

(2) DiSalvo, F. J. Challenges and opportunities in solid-state chemistry. *Pure and Applied Chemistry* **2000**, *72* (10), 1799-1807.

(3) Kanatzidis, M. G.; Poeppelmeier, K. R.; Bobev, S.; Guloy, A. M.; Hwu, S.-J.; Lachgar, A.; Latturner, S. E.; Raymond; Schaak, E.; Seo, D.-K.; et al. Report from the third workshop on future directions of solid-state chemistry: The status of solid-state chemistry and its impact in the physical sciences. *Progress in Solid State Chemistry* **2008**, *36* (1), 1-133.

(4) Phelan, W. A.; Menard, M. C.; Kangas, M. J.; McCandless, G. T.; Drake, B. L.; Chan, J. Y. Adventures in Crystal Growth: Synthesis and

Characterization of Single Crystals of Complex Intermetallic Compounds. *Chemistry of Materials* **2012**, *24* (3), 409-420.

(5) Bugaris, D. E.; zur Loye, H.-C. Materials Discovery by Flux Crystal Growth: Quaternary and Higher Order Oxides. *Angewandte Chemie International Edition* **2012**, *51* (16), 3780-3811.

(6) Moliner, M.; Rey, F.; Corma, A. Towards the Rational Design of Efficient Organic Structure-Directing Agents for Zeolite Synthesis. *Angewandte Chemie International Edition* **2013**, *52* (52), 13880-13889.

(7) Fenton, J. L.; Steimle, B. C.; Schaak, R. E. Tunable intraparticle frameworks for creating complex heterostructured nanoparticle libraries. *Science* **2018**, *360* (6388), 513-517.

(8) Goodenough, J. B.; Park, K.-S. The Li-Ion Rechargeable Battery: A Perspective. *Journal of the American Chemical Society* **2013**, *135* (4), 1167-1176.

(9) Manthiram, A.; Yu, X.; Wang, S. Lithium battery chemistries enabled by solid-state electrolytes. *Nature Reviews Materials* **2017**, *2* (4), 16103.

(10) Whittingham, M. S. Electrical Energy Storage and Intercalation Chemistry. *Science* **1976**, *192* (4244), 1126-1127.

(11) Wilson, S. T.; Lok, B. M.; Messina, C. A.; Cannan, T. R.; Flanigen, E. M. Aluminophosphate molecular sieves: a new class of microporous crystalline inorganic solids. *Journal of the American Chemical Society* **1982**, *104* (4), 1146-1147.

(12) Lobo, R. F.; Zones, S. I.; Davis, M. E. Structure-direction in zeolite synthesis. *Journal of inclusion phenomena and molecular recognition in chemistry* **1995**, *21* (1), 47-78.

(13) Park, M. B.; Jo, D.; Jeon, H. C.; Nicholas, C. P.; Lewis, G. J.; Hong, S. B. Zeolite Synthesis from a Charge Density Perspective: The Charge Density Mismatch Synthesis of UZM-5 and UZM-9. *Chemistry of Materials* **2014**, *26* (23), 6684-6694.

(14) Lee, M. M.; Teuscher, J.; Miyasaka, T.; Murakami, T. N.; Snaith, H. J. Efficient Hybrid Solar Cells Based on Meso-Superstructured Organometal Halide Perovskites. *Science* **2012**, *338* (6107), 643-647.

(15) Burschka, J.; Pellet, N.; Moon, S.-J.; Humphry-Baker, R.; Gao, P.; Nazeeruddin, M. K.; Grätzel, M. Sequential deposition as a route to high-performance perovskite-sensitized solar cells. *Nature* **2013**, *499* (7458), 316-319.

(16) Green, M. A.; Ho-Baillie, A.; Snaith, H. J. The emergence of perovskite solar cells. *Nature Photonics* **2014**, *8* (7), 506-514.

(17) Kanatzidis, M. G. Discovery-Synthesis, Design, and Prediction of Chalcogenide Phases. *Inorganic Chemistry* **2017**, *56* (6), 3158-3173.

(18) Sheldrick, W. S. Polychalcogenides. In *Handbook of Chalcogen Chemistry: New Perspectives in Sulfur, Selenium and Tellurium, Volume 1*, Wickleder, M. S., Devillanova, F., Du Mont, W.-W., Devillanova, F., Du Mont, W.-W. Eds.; Vol. 1; The Royal Society of Chemistry, 2013; p 0.

(19) Koscielski, L. A.; Ibers, J. A. The Structural Chemistry of Quaternary Chalcogenides of the Type AMM'Q3. *Zeitschrift für anorganische und allgemeine Chemie* **2012**, *638* (15), 2585-2593.

(20) Ablekim, T.; Duenow, J. N.; Zheng, X.; Moutinho, H.; Moseley, J.; Perkins, C. L.; Johnston, S. W.; O'Keefe, P.; Colegrove, E.; Albin, D. S.; et al. Thin-Film Solar Cells with 19% Efficiency by Thermal Evaporation of CdSe and CdTe. *ACS Energy Letters* **2020**, *5* (3), 892-896.

(21) Wu, X. High-efficiency polycrystalline CdTe thin-film solar cells. *Solar Energy* **2004**, *77* (6), 803-814.

(22) Hodges, J. M.; Xia, Y.; Malliakas, C. D.; Alexander, G. C. B.; Chan, M. K. Y.; Kanatzidis, M. G. Two-Dimensional CsAg5Te3–xSx Semiconductors: Multi-anion Chalcogenides with Dynamic Disorder and Ultralow Thermal Conductivity. *Chemistry of Materials* **2018**, *30* (20), 7245-7254.

(23) Hodges, J. M.; Xia, Y.; Malliakas, C. D.; Slade, T. J.; Wolverton, C.; Kanatzidis, M. G. Mixed-Valent Copper Chalcogenides: Tuning Structures and Electronic Properties Using Multiple Anions. *Chemistry of Materials* **2020**, *32* (23), 10146-10154.

(24) Dey, T.; Mumbaraddi, D.; Wen, F.; Mishra, V.; Michaelis, V. K.; Mar, A. Are Selenides the Same as Sulfides? Structure, Spectroscopy, and Properties of Narrow-Gap Rare-Earth Semiconductors RE2Sn(S1–xSex)5 (RE = La, Ce; x = 0–0.8). *Inorganic Chemistry* **2024**, *63* (23), 10726-10736. DOI: 10.1021/acs.inorgchem.4c01362.

(25) Oxley, B. M.; Cho, J. B.; Iyer, A. K.; Waters, M. J.; He, J.; Smith, N. C.; Wolverton, C.; Gopalan, V.; Rondinelli, J. M.; Jang, J. I.; et al. Heteroanionic Control of Exemplary Second-Harmonic Generation and Phase Matchability in 1D LiAsS_{2–<i>x</i>}Se_{<i>x</i>}. *Journal of the American Chemical Society* **2022**, *144* (30), 13903-13912.

(26) Tassanov, A.; Lee, H.; Xia, Y.; Hodges, J. M. Layered NaBa2M3Q3(Q2) (M = Cu or Ag; Q = S or Se) Chalcogenides and Local Ordering in Their Mixed-Anion Compositions. *Inorganic Chemistry* **2024**.

(27) Heremans, J. P.; Cava, R. J.; Samarth, N. Tetradymites as thermoelectrics and topological insulators. *Nature Reviews Materials* **2017**, *2* (10), 17049.

(28) Ji, H.; Allred, J. M.; Fuccillo, M. K.; Charles, M. E.; Neupane, M.; Wray, L. A.; Hasan, M. Z.; Cava, R. J. Bi2Te1.6S1.4: A topological insulator in the tetradymite family. *Physical Review B* **2012**, *85* (20), 201103.

(29) Pauling, L. The formula, structure, and chemical bonding of tetradymite, Bi14Te13S8, and the phase Bi14Te15S6. *American Mineralogist* **1975**, *60* (11-12), 994-997.

(30) Zhu, T.; Hu, L.; Zhao, X.; He, J. New Insights into Intrinsic Point Defects in V2VI3 Thermoelectric Materials. *Advanced Science* **2016**, *3* (7), 1600004.

(31) Witting, I. T.; Ricci, F.; Chasapis, T. C.; Hautier, G.; Snyder, G. J. The Thermoelectric Properties of n-Type Bismuth Telluride: Bismuth Selenide Alloys Bi2Te3−xSex. *Research* **2020**, *2020*.

(32) Witting, I. T.; Chasapis, T. C.; Ricci, F.; Peters, M.; Heinz, N. A.; Hautier, G.; Snyder, G. J. The Thermoelectric Properties of Bismuth Telluride. *Advanced Electronic Materials* **2019**, *5* (6), 1800904.

(33) Xiong, Y.; Yang, Y.; Joress, H.; Padgett, E.; Gupta, U.; Yarlagadda, V.; Agyeman-Budu, D. N.; Huang, X.; Moylan, T. E.; Zeng, R.; et al. Revealing the atomic ordering of binary intermetallics using in situ heating techniques at multilength scales. *Proceedings of the National Academy of Sciences* **2019**, *116* (6), 1974-1983.

(34) Almoussawi, B.; Kageyama, H.; Roussel, P.; Kabbour, H. Versatile Interplay of Chalcogenide and Dichalcogenide Anions in the Thiovanadate Ba7S(VS3O)2(S2)3 and Its Selenide Derivatives: Elaboration and DFT Meta-GGA Study. *ACS Organic & Inorganic Au* **2023**, *3* (3), 158-170.

(35) Ubukata, H.; Takeiri, F.; Shitara, K.; Tassel, C.; Saito, T.; Kamiyama, T.; Broux, T.; Kuwabara, A.; Kobayashi, G.; Kageyama, H. Anion ordering enables fast H^{−} conduction at low temperatures. *Science Advances* **2021**, *7* (23), eabf7883.

(36) Lakshan, A.; Koley, B.; Buxi, K.; Raghuvanshi, P. R.; Nuss, J.; Bhattacharya, A.; Chatterjee, R.; Roy, A.; Jana, P. P. Disorder-Mediated Structural Transformation in the Cu4TiSe4–xSx (0 ≤ x ≤ 4) System and Its Effects on the Thermal Transport Property. *Chemistry of Materials* **2024**, *36* (11), 5741-5752.

(37) Kageyama, H.; Ogino, H.; Zhu, T.; Hasegawa, T. *Mixed-anion Compounds*; Royal Society of Chemistry, 2024.

(38) Harada, J. K.; Charles, N.; Poeppelmeier, K. R.; Rondinelli, J. M. Heteroanionic Materials by Design: Progress Toward Targeted Properties. *Advanced Materials* **2019**, *31* (19), 1805295.

(39) Yang, M.; Oró-Solé, J.; Rodgers, J. A.; Jorge, A. B.; Fuertes, A.; Attfield, J. P. Anion order in perovskite oxynitrides. *Nature Chemistry* **2011**, *3* (1), 47-52.

(40) Bader, R. F. W. A Bond Path: A Universal Indicator of Bonded Interactions. *The Journal of Physical Chemistry A* **1998**, *102* (37), 7314-7323.

(41) Hume-Rothery, W. Researches on the nature, properties, and conditions of formation of intermetallic compounds, with special reference to certain compounds of tin. University of London, 1926.

(42) Ma, N.; Li, Y.-Y.; Chen, L.; Wu, L.-M. α-CsCu5Se3: Discovery of a Low-Cost Bulk Selenide with High Thermoelectric Performance. *Journal of the American Chemical Society* **2020**, *142* (11), 5293-5303.

(43) Lin, H.; Tan, G.; Shen, J.-N.; Hao, S.; Wu, L.-M.; Calta, N.; Malliakas, C.; Wang, S.; Uher, C.; Wolverton, C.; et al. Concerted Rattling in CsAg5Te3 Leading to Ultralow Thermal Conductivity and High Thermoelectric Performance. *Angewandte Chemie International Edition* **2016**, *55* (38), 11431-11436.

(44) Li, F.; Liu, X.; Ma, N.; Yang, Y.-C.; Yin, J.-P.; Chen, L.; Wu, L.-M. Overdamped Phonon Diffusion and Nontrivial Electronic Structure Leading to a High Thermoelectric Figure of Merit in KCu5Se3. *Journal of the American Chemical Society* **2023**, *145* (27), 14981-14993.

(45) Sommer, H.; Hoppe, R. Die Kristallstruktur von Cs2S. mit einer Bemerkung über Cs2Se, Cs2Te, Rb2Se und Rb2Te. *Zeitschrift für anorganische und allgemeine Chemie* **1977**, *429* (1), 118-130.

(46) Moëlo, Y.; Popa, A. F.; Dubost, V. The bond valence model as a prospective approach: examination of the crystal structures of copper chalcogenides with Cu bond valence excess. *Acta Crystallographica Section B* **2022**, *78* (4), 627-636.

(47) Adams, S. Practical Considerations in Determining Bond Valence Parameters. In *Bond Valences*, Brown, I. D., Poeppelmeier, K. R. Eds.; Springer Berlin Heidelberg, 2014; pp 91-128.

(48) Tang, W.; Sanville, E.; Henkelman, G. A grid-based Bader analysis algorithm without lattice bias. *Journal of Physics: Condensed Matter* **2009**, *21* (8), 084204.

(49) Allred, A. L. Electronegativity values from thermochemical data. *Journal of Inorganic and Nuclear Chemistry* **1961**, *17* (3), 215-221.

(50) Zhang, H.; Huang, W.; Wang, W.-C.; Shi, X.-Q. Ionicity of bonding in elemental solids. *Journal of Physics Communications* **2018**, *2* (11), 115009.

(51) Shannon, R. D.; Prewitt, C. T. Effective ionic radii in oxides and fluorides. *Acta Crystallographica Section B* **1969**, *25* (5), 925-946.

(52) Bragg, W. L.; Williams, E. J. The effect of thermal agitation on atomic arrangement in alloys. *Proceedings of the Royal Society of London. Series A, Containing Papers of a Mathematical and Physical Character* **1934**, *145* (855), 699-730.

(53) Santodonato, L. J.; Liaw, P. K.; Unocic, R. R.; Bei, H.; Morris, J. R. Predictive multiphase evolution in Al-containing high-entropy alloys. *Nature Communications* **2018**, *9* (1), 4520.

(54) Santodonato, L. J.; Zhang, Y.; Feygenson, M.; Parish, C. M.; Gao, M. C.; Weber, R. J. K.; Neuefeind, J. C.; Tang, Z.; Liaw, P. K. Deviation from high-entropy configurations in the atomic distributions of a multi-principal-element alloy. *Nature Communications* **2015**, *6* (1), 5964.

(55) Assadi, H.; Greer, A. L. Site-ordering effects on element partitioning during rapid solidification of alloys. *Nature* **1996**, *383* (6596), 150-152.

(56) Nakatsuka, S.; Nose, Y. Order–Disorder Phenomena and Their Effects on Bandgap in ZnSnP2. *The Journal of Physical Chemistry C* **2017**, *121* (2), 1040-1046.

(57) Iglesias, J. E.; Pachali, K. E.; Steinfink, H. The crystal structures and phase transition of α and β BaCu4S3. *Materials Research Bulletin* **1972**, *7* (11), 1247-1258.

(58) Zong, P.-a.; Kimata, K.; Li, Z.; Zhang, P.; Liang, J.; Wan, C.; Koumoto, K. A p-type thermoelectric material BaCu4S3 with high electronic band degeneracy. *Journal of Applied Physics* **2019**, *126* (2). DOI: 10.1063/1.5099291 (acccessed 7/27/2024).

(59) Mansuetto, M. F.; Keane, P. M.; Ibers, J. A. Synthesis and Structures of the New Group IV Chalcogenides NaCuTiS3 and NaCuZrQ3 (Q = S, Se, Te). *Journal of Solid State Chemistry* **1993**, *105* (2), 580-587.

(60) Wang, J.; Greenfield, J. T.; Kovnir, K. Synthesis, crystal structure, and magnetic properties of quaternary iron selenides: Ba2FePnSe5 (Pn=Sb, Bi). *Journal of Solid State Chemistry* **2016**, *242*, 22-27.

(61) Geng, L.; Cheng, W.-D.; Zhang, H.; Lin, C.-S.; Zhang, W.-L.; Li, Y.-Y.; He, Z.-Z. Syntheses, Crystal and Electronic Structures, and Characterizations of Quaternary Antiferromagnetic Sulfides: Ba2MFeS5 (M = Sb, Bi). *Inorganic Chemistry* **2011**, *50* (6), 2378-2384.

(62) Mansuetto, M. F.; Keane, P. M.; Ibers, J. A. Synthesis, structure, and conductivity of the new group IV chalcogenides, KCuZrQ3 (Q = S, Se, Te). *Journal of Solid State Chemistry* **1992**, *101* (2), 257-264.

(63) Hohenberg, P.; Kohn, W. Inhomogeneous Electron Gas. *Physical Review* **1964**, *136* (3B), B864-B871.

(64) Kresse, G.; Hafner, J. Ab initio molecular dynamics for liquid metals. *Physical Review B* **1993**, *47* (1), 558-561.

(65) Kresse, G.; Hafner, J. Ab initio molecular-dynamics simulation of the liquid-metal--amorphous-semiconductor transition in germanium. *Physical Review B* **1994**, *49* (20), 14251-14269.

(66) Kresse, G.; Furthmüller, J. Efficiency of ab-initio total energy calculations for metals and semiconductors using a plane-wave basis set. *Computational Materials Science* **1996**, *6* (1), 15-50.

(67) Blöchl, P. E. Projector augmented-wave method. *Physical Review B* **1994**, *50* (24), 17953-17979.

(68) Perdew, J. P.; Burke, K.; Wang, Y. Generalized gradient approximation for the exchange-correlation hole of a many-electron system. *Physical Review B* **1996**, *54* (23), 16533-16539.

TOC

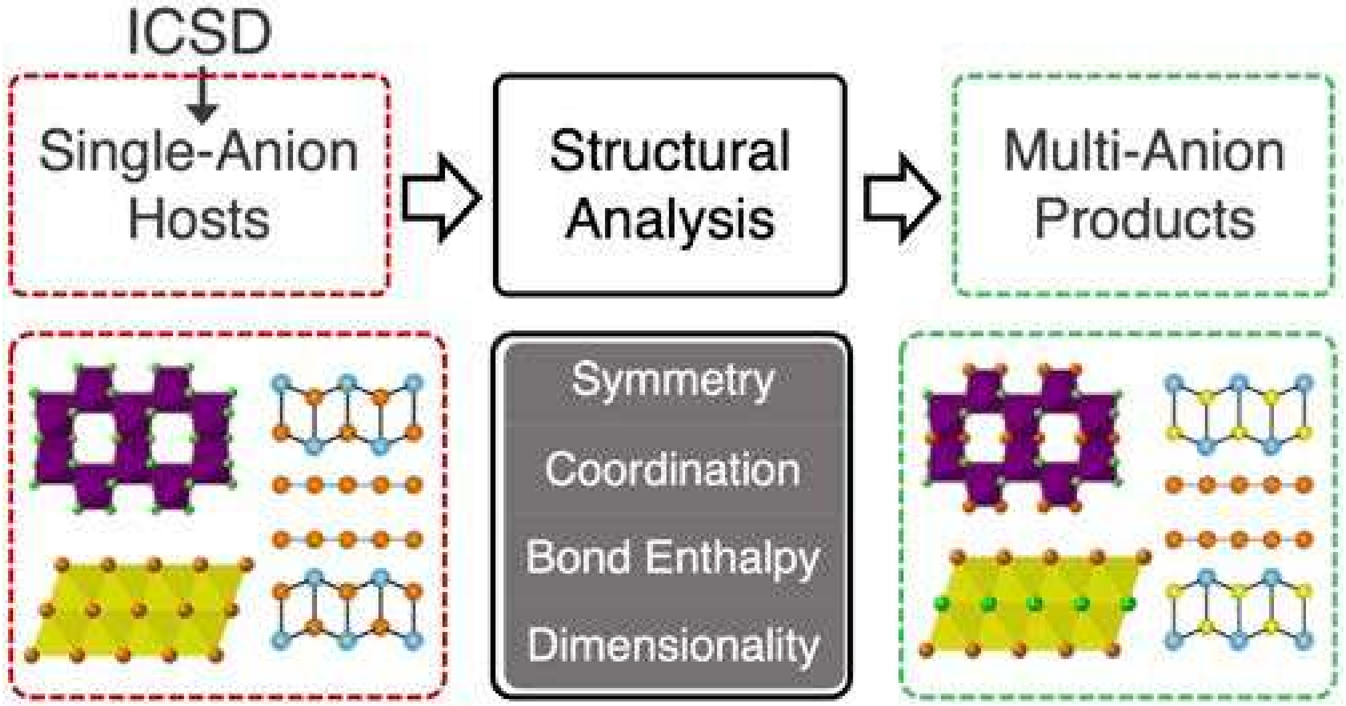
ICSD
Single-Anion Hosts
Structural Analysis
Multi-Anion Products
Symmetry
Coordination
Bond Enthalpy
Dimensionality